Monatshefte für Chemie 138, 381–388 (2007)
DOI 10.1007/s00706-007-0597-2
Printed in The Netherlands

Monatshefte für Chemie
Chemical Monthly

The Stannides YNi_xSn_2 ($x = 0$, 0.14, 0.21, 1) – Syntheses, Structure, and ^{119}Sn *Mössbauer* Spectroscopy

C. Peter Sebastian and **Rainer Pöttgen***

Institut für Anorganische und Analytische Chemie and NRW Graduate School of Chemistry, Westfälische Wilhelms-Universität Münster, Münster, Germany

Received July 4, 2006; accepted (revised) August 21, 2006; published online February 22, 2007

Summary. The stannides YNi_xSn_2 ($x = 0$, 0.14, 0.21, 1) were prepared by arc-melting of the pure elements. They were characterized through X-ray powder and single crystal data: $ZrSi_2$ type, space group *Cmcm*, $a = 438.09(6)$, $b = 1629.6(4)$, $c = 430.34(7)$ pm, $wR2 = 0.0607$, 386 F^2 values, 14 variables for YSn_2, $CeNiSi_2$ type, *Cmcm*, $a = 440.6(1)$, $b = 1640.3(1)$, $c = 433.0(1)$ pm, $wR2 = 0.0632$, 416 F^2 values, 19 variables for $YNi_{0.142(7)}Sn_2$, $a = 441.0(1)$, $b = 1646.3(1)$, $c = 434.6(1)$ pm, $wR2 = 0.0491$, 287 F^2 values, 19 variables for $YNi_{0.207(7)}Sn_2$, and $LuNiSn_2$ type, space group *Pnma*, $a = 1599.3(3)$, $b = 440.89(5)$, $c = 1456.9(2)$ pm, $wR2 = 0.0375$, 1538 F^2 values, 74 variables for $YNiSn_2$. The YSn_2 structure contains Sn1–Sn1 zig-zag chains (297 pm) and planar Sn2 networks (307 pm). The stannides $YNi_{0.142(7)}Sn_2$ and $YNi_{0.207(7)}Sn_2$ are nickel filled versions of YSn_2. The nickel atoms have a distorted pyramidal tin coordination with Ni–Sn distances ranging from 220 to 239 pm. New stannide $YNiSn_2$ adopts the $LuNiSn_2$ type. The nickel and tin atoms build up a complex three-dimensional $[NiSn_2]$ network in which the yttrium atoms fill distorted pentagonal and hexagonal channels. Within the network all nickel atoms have a distorted square pyramidal tin coordination with Ni–Sn distances ranging from 247 to 276 pm. Except the Sn4 atoms which are located in a tricapped trigonal Y_6 prism, all tin atoms have between 4 and 5 tin neighbors between 297 and 350 pm. ^{119}Sn *Mössbauer* spectroscopic data of YNi_xSn_2 show a decreasing isomer shift (from 2.26 to 2.11 mm/s) from YSn_2 to $YNiSn_2$, indicating decrease of the *s* electron density at the tin nuclei.

Keywords. Stannides; Intermetallics; *Mössbauer* spectroscopy.

* Corresponding author. E-mail: pottgen@uni-muenster.de

Introduction

^{119}Sn *Mössbauer* spectroscopy is a useful tool for studying the electronic situation and the chemical bonding in tin based *Zintl* phases and intermetallic compounds [1–3]. The isomer shift δ arises from the electrostatic interaction between nuclear and electron charge distributions due to the finite size of the nucleus. δ is influenced by changes of the nuclear radius as well as the electron density at the nucleus. From a structural point of view, changes of the electron density at the nucleus are related to changes in the local near neighbor coordination. Thus δ gives valuable information on changes in the chemical bonding.

Systematic studies on the tin isomer shifts have been performed for many complex chalcogenides [3] and chalcogen containing *Zintl* phases [4]. In intermetallic stannides variation of δ can be due to (i) differences in the electron count or (ii) electronegativity differences. Recent examples for the influence *via* the electron count are the stannides $CaTSn_2$ (T = Rh, Pd, Ir) [5] and $AuTSn_2$ (T = Ni, Cu, Pd) [6]. In both series $CaPdSn_2$ and $AuCuSn_2$ show higher isomer shifts, indicating a higher *s* electron density at the tin nuclei. Similar behavior was demonstrated for the binary palladium stannides $PdSn_2$, $PdSn_3$, and $PdSn_4$ [7, 8]. With increasing tin content the more electronegative palladium atoms have less influence on the tin nuclei. Consequently, the *s* electron density

and the isomer shifts increase. In the *RET*Sn series (*RE* = rare earth element, *T* = Cu, Ag, Au) [9–11, and Refs. therein] the ^{119}Sn isomer shifts continuously decrease from the lanthanum to the lutetium compound. Since the electronegativity of the *RE* element increases in the same direction, less electron density is transferred from the rare earth metal component to the [*T*Sn] network and the *s* electron density at the tin nuclei decreases.

We have now tested this approach for the series of YNi_xSn_2 ($x = 0$, 0.1, 0.2, 1) stannides. So far only X-ray powder data have been reported for YSn_2 [12–14]. The nickel containing stannides are reported here for the first time. Herein we report on a full crystallographic and *Mössbauer* spectroscopic characterization of these materials.

Discussion

Crystal Chemistry

The crystal structures of YNi_xSn_2 ($x = 0$, 0.14, 0.21, 1) have been refined from single crystal diffractometer data. For $ZrSi_2$ type YSn_2 only X-ray powder data had been reported [12–14]. The nickel containing stannides are reported here for the first time. The structures of YSn_2 and $YNi_{0.142}Sn_2$ are presented in Fig. 1. The Sn1 atoms have trigonal prismatic yttrium coordination in both stannides. These trigonal prisms are condensed *via* common rectangular faces building two-dimensional blocks which extend in the *xz* plane. The Sn1 atoms have two further Sn1 neighbors in the adjacent prisms leading to zig-zag chains with Sn1–Sn1 distances of 297 pm in both compounds. These Sn–Sn distances are between those in α-(4 × 281 pm) and β-tin (4 × 302 and 2 × 318 pm) [22]. Between these AlB_2 related slabs we observe planar networks formed by the Sn2 atoms. Here, each Sn2 atom has four Sn2 neighbors at Sn2–Sn2 of 307, 309, and 310 pm in YSn_2, $YNi_{0.142}Sn_2$, and $YNi_{0.207}Sn_2$, slightly longer than in the AlB_2 slabs.

The nickel atoms in the nickel containing stannides are located in distorted square pyramidal tin voids (Fig. 1). Refinement of the occupancy parameters revealed the compositions $YNi_{0.142}Sn_2$ and $YNi_{0.207}Sn_2$. We had also prepared samples in the series YNi_xSn_2 with higher nickel contents, however, refinement of the crystal structures revealed that the maximum nickel occupancy was around 20%, leading to a rather small homogeneity range. For many other stannides $RET_{1-x}Sn_2$ similar small transition metal contents have been observed [23]. Different to $YNi_{0.142}Sn_2$ and $YNi_{0.207}Sn_2$, the stannides $CeMn_{0.4}Sn_{1.9}$,

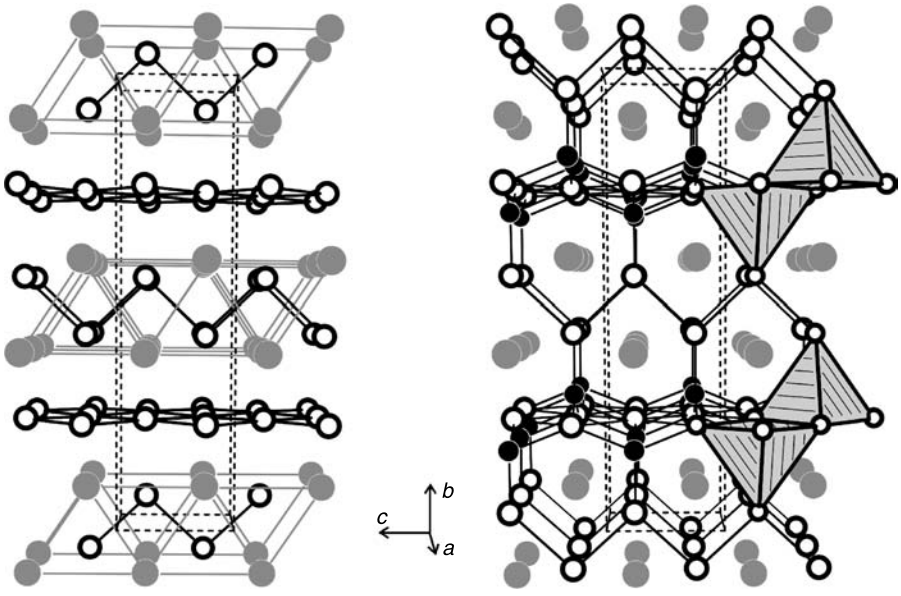

Fig. 1. The crystal structures of YSn_2 (left-hand drawing) and $YNi_{0.14}Sn_2$. Yttrium, nickel, and tin atoms are drawn as medium gray, filled, and open circles. The AlB_2 related substructure and the planar networks of the Sn2 atoms in YSn_2 are emphasized. In the right-hand drawing the three-dimensional $[Ni_{0.14}Sn_2]$ network and the pyramidal nickel coordination of $YNi_{0.14}Sn_2$ are highlighted

$NdCo_{0.9}Sn_{1.4}$, and $NdCo_{0.30}Sn_{1.72}$ [23] additionally revealed defects on the tin sites. The refined compositions of the two investigated single crystals do not exactly fit the starting compositions used during the synthesis procedure. Such behavior is often observed for crystals that originate from samples with small homogeneity ranges.

The Ni–Sn distances within the three-dimensional $[Ni_{0.142}Sn_2]$ and $[Ni_{0.207}Sn_2]$ networks range from 220 to 239 pm, somewhat smaller than the sum of the covalent radii [24] of 255 pm. This is understandable in view of the small partial nickel occupancy. With increasing nickel content, the YSn_2 substructure is slightly expanded leaving larger voids for the nickel atoms and consequently longer Ni–Sn distances. Such a behavior has also been observed for other $CeNiSi_2$ related intermetallics [25–32] as well as for a series of rare earth-transition metal indides $RE_{10}Rh_{9-x}In_{20}$ [33].

In line with these partial occupancies are the slightly enhanced U_{22} values of the Sn1 atoms in $YNi_{0.142}Sn_2$ and $YNi_{0.207}Sn_2$. These displacements go *via* the square pyramidal voids. Similar behavior has been observed for the isotypic stannides $LaCu_{0.56}Sn_2$, $LaNi_{0.74}Sn_2$, $LaCo_{0.52}Sn_2$, and $LaFe_{0.34}Sn_2$ [25]. Among the more than 80 intermetallics [26] that crystallize with the $CeNiSi_2$ type structure [18], especially the germanides and stannides [27–32] reveal only partial filling of the square pyramidal voids. Full occupancy of the transition metal site has for example been observed for $EuIrGe_2$ [34]. The square pyramidal voids also occur in the well known $ThCr_2Si_2$ structure [35], and consequently the $CeNiSi_2$ type can be considered as a 1:1 intergrowth variant [36–38] of slightly distorted AlB_2 and $ThCr_2Si_2$ related slabs.

Finally we draw back to the cell volumes. With increasing nickel content the unit cell parameters isotropically increase from YSn_2 to $YNi_{0.207}Sn_2$ (Table 1). In $YNiSn_2$ with the highest nickel content, the cell volume of one third of the cell (for $Z = 4$) is $0.3424\,nm^3$.

The structure of $YNiSn_2$ is somewhat more complex. It contains three yttrium, three nickel, and six

Table 1. Crystal data and structure refinement for YNi_xSn_2 ($x = 0$, 0.142, 0.207, 1)

Empirical formula	YSn_2	$YNi_{0.142}Sn_2$	$YNi_{0.207}Sn_2$	$YNiSn_2$
Formula mass	329.29	334.66	338.47	385.00
Structure type	$ZrSi_2$	$CeNiSi_2$	$CeNiSi_2$	$LuNiSn_2$
Instrument	IPDS II	CAD4	CAD4	IPDS II
Unit cell dimensions	$a = 438.09(6)$ pm	$a = 440.6(1)$ pm	$a = 441.0(1)$ pm	$a = 1599.3(3)$ pm
	$b = 1629.6(4)$ pm	$b = 1640.3(1)$ pm	$b = 1646.3(1)$ pm	$b = 440.89(5)$ pm
	$c = 430.34(7)$ pm	$c = 433.0(1)$ pm	$c = 434.6(1)$ pm	$c = 1456.9(2)$ pm
	$V = 0.3072\,nm^3$	$V = 0.3129\,nm^3$	$V = 0.3155\,nm^3$	$V = 1.0273\,nm^3$
Z	4	4	4	12
Space group	*Cmcm*	*Cmcm*	*Cmcm*	*Pnma*
Calculated density	$7.05\,g/cm^3$	$7.10\,g/cm^3$	$7.13\,g/cm^3$	$7.47\,g/cm^3$
Crystal size	$10 \times 50 \times 110\,\mu m^3$	$45 \times 45 \times 90\,\mu m^3$	$25 \times 45 \times 65\,\mu m^3$	$20 \times 40 \times 40\,\mu m^3$
Transm. ratio (max/min)	4.39	1.63	1.61	1.29
Absorption coefficient	$34.5\,mm^{-1}$	$34.7\,mm^{-1}$	$34.8\,mm^{-1}$	$36.3\,mm^{-1}$
$F(000)$	556	572	579	2004
θ range	4°–34°	2°–35°	2°–30°	1°–30°
Range in *hkl*	±6, −21/+25, ±6	±7, ±26, ±6	±6, ±22, ±6	±21, −6/+5, ±19
Total no. reflections	2196	2682	1798	9181
Independent reflections	386 ($R_{int} = 0.0444$)	416 ($R_{int} = 0.0662$)	287 ($R_{int} = 0.0639$)	1538 ($R_{int} = 0.0374$)
Reflections with $I > 2\sigma(I)$	350 ($R_{sigma} = 0.0246$)	355 ($R_{sigma} = 0.0319$)	253 ($R_{sigma} = 0.0359$)	1392 ($R_{sigma} = 0.0230$)
Data/parameters	386/14	416/19	287/19	1538/74
Goodness-of-fit on F^2	1.064	1.178	1.195	1.274
Final R indices [$I > 2\sigma(I)$]	$R1 = 0.0245$	$R1 = 0.0329$	$R1 = 0.0249$	$R1 = 0.0267$
	$wR2 = 0.0597$	$wR2 = 0.0604$	$wR2 = 0.0478$	$wR2 = 0.0367$
R indices (all data)	$R1 = 0.0278$	$R1 = 0.0420$	$R1 = 0.0303$	$R1 = 0.0325$
	$wR2 = 0.0607$	$wR2 = 0.0632$	$wR2 = 0.0491$	$wR2 = 0.0375$
Extinction coefficient	0.0105(7)	0.021(1)	0.0156(7)	0.00141(7)
Largest diff. peak and hole	1.56 and $-2.12\,e/Å^3$	3.65 and $-3.19\,e/Å^3$	2.92 and $-2.60\,e/Å^3$	1.26 and $-1.51\,e/Å^3$

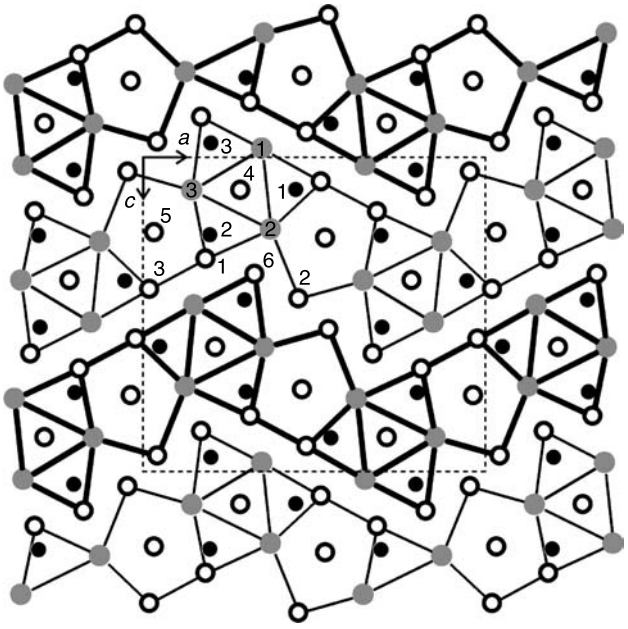

Fig. 2. Projection of the $YNiSn_2$ structure onto the *xz* plane. Yttrium, nickel, and tin atoms are drawn as gray, filled, and open circles, respectively. All atoms lie on mirror planes at $y = 1/4$ (thin lines) and $y = 3/4$ (thick lines). The trigonal and pentagonal prismatic subunits around the nickel and tin positions are emphasized

crystallographically independent tin sites. To the best of our knowledge, $YNiSn_2$ is reported here for the first time. $YNiSn_2$ has been listed in Ref. [23], however, with the same lattice parameters as the prototype $LuNiSn_2$. This is most likely a printing error. Our structure refinement fully confirmed the prototype, but the crystallographic data on $YNiSn_2$ are more precise, since the $LuNiSn_2$ structure had been refined on the basis of *Weissenberg* film data.

Figure 2 shows a projection of the $YNiSn_2$ structure onto the *xz* plane. The three crystallographically independent nickel atoms fill trigonal prismatic voids formed by yttrium and tin atoms. Together with the Sn4 centered Y_6 prism they build up a unit of four condensed trigonal prisms. The Sn5 atoms have a distorted pentagonal prismatic coordination by four yttrium and six tin atoms. These pentagonal prisms are condensed with the trigonal prisms building the basic structural unit of $YNiSn_2$. These units build layers that extend in the *xy* plane. Adjacent layers are shifted with respect to each other by half a translation period *y* as emphasized by thin and thick lines in Fig. 2. All rectangular faces of the trigonal and the pentagonal prisms are capped by further yttrium, nickel, or tin atoms, leading to coordination numbers 9 (Ni1, Ni2, Ni3, Sn4) and 15 (Sn5).

The shortest interatomic distances in the $YNiSn_2$ structure occur between the nickel and tin atoms. The Ni–Sn distances range from 247 to 276 pm, close to the sum of the covalent radii [24] of 255 pm. We can thus assume significant Ni–Sn bonding in $YNiSn_2$. The Ni–Sn distances in $YNiSn_2$ are longer than in $YNi_{0.142}Sn_2$ and $YNi_{0.207}Sn_2$, since we observe full nickel occupancy. Except the *isolated* Sn4 atoms (see Fig. 2) we observe a variety of Sn–Sn interactions for the species Sn1, Sn2, Sn3, Sn5, and Sn6. The many Sn–Sn distances cover the broad range from 297 to 350 pm, comparable to YSn_2 and the tin modifications discussed above. Together the nickel and tin atoms build up a complex three-dimensional $[NiSn_2]$ network in which the yttrium atoms fill distorted pentagonal or hexagonal channels (Fig. 3).

Similar to $YNi_{0.142}Sn_2$ and $YNi_{0.207}Sn_2$, also the nickel atoms in $YNiSn_2$ have a slightly distorted square pyramidal tin coordination. As emphasized in Fig. 4, these square pyramides are condensed *via* common corners and edges leading to a complex three-dimensional arrangement which leaves voids for the yttrium coordination. For a more detailed

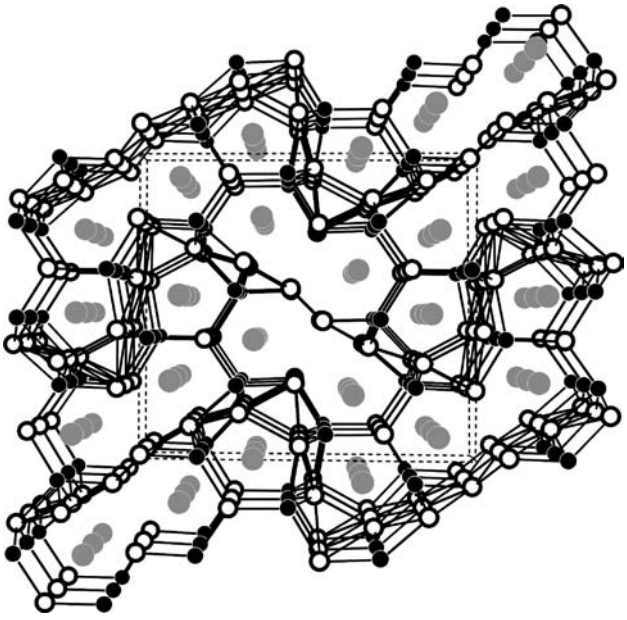

Fig. 3. View of the $YNiSn_2$ structure approximately along the *y* axis. Yttrium, nickel, and tin atoms are drawn as medium gray, filled, and open circles. The three-dimensional $[NiSn_2]$ network is emphasized. All Ni–Sn and Sn–Sn bonds up to 278 and 348 pm, respectively, are drawn

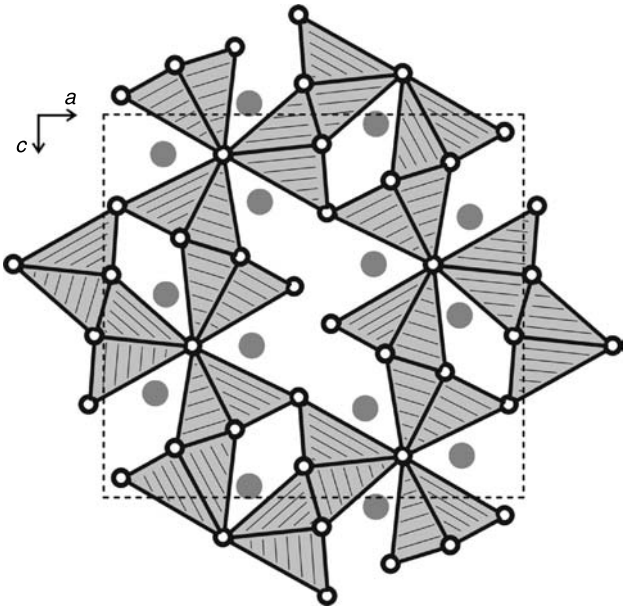

Fig. 4. Projection of the $YNiSn_2$ structure along the *y* axis. Yttrium and tin atoms are drawn as medium grey and open circles. The network of condensed $NiSn_5$ pyramids is emphasized

discussion of the different coordination polyhedra in this structure type we refer to the previous work [19, 23].

^{119}Sn Mössbauer Spectroscopy

The ^{119}Sn *Mössbauer* spectra of the YNi_xSn_2 ($x = 0$, 0.1, 0.2, 1) samples are shown in Fig. 5 together with transmission integral fits. The corresponding fitting parameters are listed in Table 5. As expected from the non-cubic site symmetry of the four stannides, the spectra show significant quadrupole splitting. The six crystallographically independent tin sites in $YNiSn_2$ cannot be resolved in the ^{119}Sn spectrum. The similar lines are superimposed, leading to a slightly higher experimental line width. The isomer shifts decrease from 2.26 mm/s (YSn_2) to 2.11 mm/s ($YNiSn_2$). Due to the increasing nickel content, *s* electron density is removed from the tin nuclei, similar to the series $CaTSn_2$ (T = Rh, Pd, Ir) [5] and $AuTSn_2$ (T = Ni, Cu, Pd) [6]. Although the isomer shifts have standard deviations up to 0.08 mm/s, the trend in the shifts is significant at least within the series of filled YSn_2 stannides. Due to the superposition of the six signals for $YNiSn_2$, comparison with the YNi_xSn_2 data should not be overinterpreted.

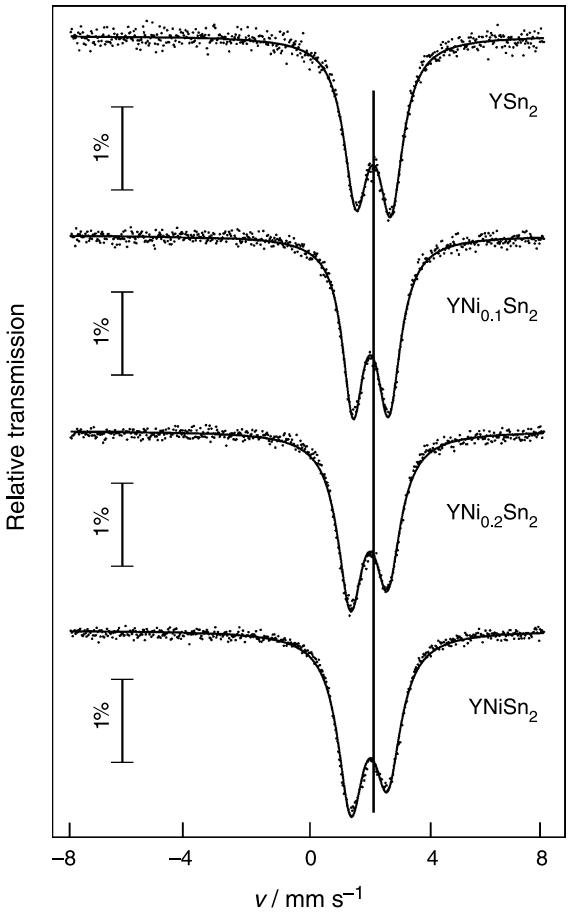

Fig. 5. ^{119}Sn *Mössbauer* spectra of the YNi_xSn_2 ($x = 0$, 0.1, 0.2, 1) samples at 78 K. The medium gray line serves as a guide for the eye in order to see the shift of the signals. For details see text

Experimental

Synthesis

Starting materials for the preparation of the YNi_xSn_2 ($x = 0$, 0.1, 0.2, 1) stannides were yttrium ingots (Johnson Matthey), nickel wire (Johnson Matthey), and tin granules (Merck), all with stated purities better than 99.9%. In a first step the larger yttrium ingots were cut into smaller pieces and the latter were arc-melted [15] to small buttons under Ar. Ar was purified before over Ti sponge (900 K), silica gel, and molecular sieves. The pre-melting procedure strongly reduces shattering during the subsequent reactions with nickel and tin.

The Y buttons, pieces of the Ni wire, and the Sn granules were then weighed in the ideal YNi_xSn_2 ($x = 0$, 0.1, 0.2, 0.4, 0.7, 1) atomic ratios and arc-melted. All samples were turned over and re-melted three times in order to ensure homogeneity. The total weight loss after the different melting procedures was smaller than 0.5 wt%. The polycrystalline samples are silvery and stable in air over weeks. The single crystals exhibit metallic luster.

Scanning Electron Microscopy

The single crystals investigated on the diffractometers have been analyzed by EDX measurements using a LEICA 420 I scanning electron microscope with elemental yttrium, nickel, and tin as standards. No impurity elements were detected. Various point analyses on the crystal revealed the compositions 36 ± 2 at% Y: 64 ± 2 at% Sn for the YSn_2 crystal, 37 ± 3 at% Y: 3 ± 1 at% Ni: 60 ± 3 at% Sn for the $YNi_{0.142}Sn_2$ crystal, 32 ± 2 at% Y: 6 ± 1 at% Ni: 62 ± 2 at% Sn for the $YNi_{0.207}Sn_2$ crystal, and 29 ± 2 at% Y: 21 ± 2 at% Ni: 50 ± 2 at% Sn for the $YNiSn_2$ crystal, close to the values obtained from the structure refinements. The standard uncertainties account for the analyses at different points of the irregularly shaped crystals.

X-Ray Film Data and Structure Refinements

The samples were characterized through *Guinier* powder patterns using CuKα_1 radiation and α-quartz ($a = 491.30$, $c = 540.46$ pm) as an internal standard. The *Guinier* camera was equipped with an imaging plate system (Fujifilm BAS-1800). The orthorhombic lattice parameters (Table 1) were obtained from least-squares fits of the powder data. To ensure correct indexing, the observed powder patterns were compared with calculated ones [16] using the atomic positions obtained from the structure refinements. The lattice parameters of the crystals and the powders agreed well. For YSn_2 our lattice parameters agreed well with the data ($a = 439.4(2)$, $b = 1634.0(5)$, and $c = 430.5(2)$ pm) originally reported by *Iandelli* and *Palenzona* [12].

Irregularly shaped single crystals of the YNi_xSn_2 ($x = 0$, 0.1, 0.2, 1) stannides were selected from the arc-melted samples and first examined by *Laue* photographs on a *Buerger* precession camera (equipped with an imaging plate system Fujifilm BAS-1800) in order to establish suitability for intensity data collection. Intensity data of the $YNi_{0.142}Sn_2$ and $YNi_{0.207}Sn_2$ crystals were collected at room temperature by use of a four-circle diffractometer (CAD4) with graphite monochromatized MoK$_\alpha$ (71.073 pm) radiation and a scintillation counter with pulse height discrimination. The scans were taken in the $\omega/2\theta$ mode and empirical absorption corrections were applied on the basis of psi-scan data, followed by spherical absorption corrections. The YSn_2 and $YNiSn_2$ crystals were measured at room temperature by use of a *Stoe* IPDS-II diffractometer

Table 2. Atomic coordinates and anisotropic displacement parameters (pm^2) for YNi_xSn_2 ($x = 0$, 0.142, 0.207, 1). U_{eq} is defined as one third of the trace of the orthogonalized U_{ij} tensor. The anisotropic displacement factor exponent takes the form $-2\pi^2[(ha^*)^2U_{11} + \cdots + 2kha^*b^*U_{12}]$. $U_{12} = U_{23} = 0$

Atom	*Wyckoff* position	x	y	z	U_{11}	U_{22}	U_{33}	U_{13}	U_{eq}
YSn_2									
Y	4*c*	0	0.09939(4)	1/4	63(3)	93(3)	67(3)	0	74(2)
Sn1	4*c*	0	0.43740(3)	1/4	69(2)	159(3)	58(2)	0	95(2)
Sn2	4*c*	0	0.74850(3)	1/4	90(3)	123(3)	88(3)	0	100(2)
$YNi_{0.142(7)}Sn_2$									
Y	4*c*	0	0.09999(6)	1/4	102(4)	98(4)	112(4)	0	104(2)
Ni (14.2(7)%)	4*c*	0	0.3024(5)	1/4	97(40)	155(43)	101(44)	0	118(25)
Sn1	4*c*	0	0.43794(5)	1/4	103(3)	291(4)	110(4)	0	168(2)
Sn2	4*c*	0	0.74867(4)	1/4	173(4)	177(4)	210(5)	0	187(2)
$YNi_{0.207(7)}Sn_2$									
Y	4*c*	0	0.10037(6)	1/4	112(5)	98(5)	123(5)	0	111(3)
Ni (20.7(7)%)	4*c*	0	0.3051(4)	1/4	155(38)	172(37)	130(39)	0	152(22)
Sn1	4*c*	0	0.43860(5)	1/4	103(4)	379(6)	108(4)	0	197(3)
Sn2	4*c*	0	0.74892(5)	1/4	187(5)	223(5)	211(6)	0	207(3)
$YNiSn_2$									
Y1	4*c*	0.84929(4)	1/4	0.52714(4)	72(2)	78(3)	78(3)	4(2)	76(1)
Y2	4*c*	0.37431(4)	1/4	0.23033(5)	107(3)	92(3)	80(3)	14(2)	93(1)
Y3	4*c*	0.14483(4)	1/4	0.10660(5)	77(2)	102(3)	86(3)	−6(2)	88(1)
Ni1	4*c*	0.55152(5)	1/4	0.89532(6)	75(3)	83(4)	106(4)	−3(3)	88(2)
Ni2	4*c*	0.80286(5)	1/4	0.75116(7)	151(4)	91(4)	109(4)	46(3)	117(2)
Ni3	4*c*	0.29932(5)	1/4	0.45660(6)	83(3)	88(4)	97(4)	5(3)	90(2)
Sn1	4*c*	0.18528(3)	1/4	0.32492(3)	86(2)	81(2)	77(2)	8(2)	81(1)
Sn2	4*c*	0.45620(3)	1/4	0.45120(4)	67(2)	125(2)	183(3)	−9(2)	125(1)
Sn3	4*c*	0.02106(2)	1/4	0.42076(3)	65(2)	67(2)	93(2)	−1(1)	75(1)
Sn4	4*c*	0.71365(2)	1/4	0.89352(3)	67(2)	77(2)	78(2)	3(2)	74(1)
Sn5	4*c*	0.96605(3)	1/4	0.75902(3)	116(2)	148(2)	133(2)	37(2)	133(1)
Sn6	4*c*	0.67248(3)	1/4	0.62680(3)	99(2)	72(2)	85(2)	15(2)	86(1)

with graphite monochromatized MoKα radiation in oscillation mode. The absorption corrections were numerical. All relevant crystallographic details for the data collections and evaluations are listed in Table 1.

Careful analyses of the data sets revealed the space groups *Cmcm* for YSn_2, $YNi_{0.142}Sn_2$ and $YNi_{0.207}Sn_2$, and *Pnma* for $YNiSn_2$. The isotypy of YSn_2 with $ZrSi_2$ [17], of $YNi_{0.142}Sn_2$ and $YNi_{0.207}Sn_2$ with $CeNiSi_2$ [18], and $YNiSn_2$ with $LuNiSn_2$ [19] was already evident from the *Guinier* data. The starting atomic positions were then determined by automatic interpretations of direct methods with SHELXS-97 [20] and the four structures were refined using SHELXS-97 (full-matrix least-squares on F_o^2) [21] with anisotropic atomic displacement parameters for all sites. The nickel sites in $YNi_{0.142}Sn_2$ and $YNi_{0.207}Sn_2$ were only partially occupied and these occupancy parameters have been refined as a least-squares variable. All other sites were fully occupied within two standard uncertainties. The refinements went smoothly to the residuals listed in Table 1. The final difference *Fourier* synthesis revealed no significant residual peaks (Table 1). The positional parameters and interatomic distances are listed in Tables 2–4. Further details on the structure refinements are available. Details may be obtained from: Fachinformationszentrum Karlsruhe, 76344 Eggenstein-Leopoldshafen (Germany), by quoting the Registry Nos. CSD-416771 (YSn_2), CSD-416772 ($YNi_{0.142}Sn_2$), CSD-416773 ($YNi_{0.207}Sn_2$), and CSD-416774 ($YNiSn_2$).

Table 3. Interatomic distances (pm), calculated with the lattice parameters taken from X-ray powder data of YSn_2 and single crystal lattice parameters for YNi_xSn_2 ($x = 0.14, 0.21$). All distances within the first coordination spheres are listed. Standard deviations are equal or less than 0.8 pm

YSn_2							$YNi_{0.14}Sn_2$	$YNi_{0.21}Sn_2$
Y:	4	Sn1	312.9	Y:	4	Sn1	315.1	316.2
	2	Sn2	327.2		2	Sn2	328.6	329.3
	2	Sn2	328.2		2	Sn2	329.4	329.8
	2	Sn1	343.0		1	Ni	332.0	337.0
					2	Sn1	345.2	345.8
				Ni:	1	Sn1	222.3	219.8
					2	Sn2	232.1	234.8
					2	Sn2	237.3	239.1
					1	Y	332.0	337.0
					4	Y	347.9	346.5
Sn1:	2	Sn1	296.5	Sn1:	1	Ni	222.3	219.8
	4	Y	312.9		2	Sn1	297.2	296.8
	2	Y	343.0		4	Y	315.1	316.2
					2	Y	345.2	345.8
Sn2:	4	Sn2	307.1	Sn2:	2	Ni	232.1	234.8
	2	Y	327.2		2	Ni	237.3	239.1
	2	Y	328.2		4	Sn2	308.9	309.6
					2	Y	328.6	329.3
					2	Y	329.4	329.8

Table 4. Interatomic distances (pm) of $YNiSn_2$, calculated with the lattice parameters taken from X-ray powder data. All distances within the first coordination spheres are listed. Standard deviations are equal or less than 0.2 pm

Y1:	2	Sn4	310.8	Ni1:	2	Sn3	251.9	Sn1:	2	Ni2	247.5	Sn4:	1	Ni2	251.7
	2	Sn3	312.0		1	Sn4	259.3		1	Ni3	264.7		1	Ni3	257.8
	2	Sn1	313.2		1	Sn5	263.1		1	Sn3	297.4		1	Ni1	259.3
	1	Sn3	315.4		1	Sn3	272.4		2	Y1	313.2		2	Y1	310.8
	1	Sn6	317.9		2	Y2	310.1		2	Sn6	324.5		2	Y3	316.0
	2	Ni3	325.0		2	Y1	332.6		1	Y3	324.6		2	Y2	317.7
	2	Ni1	332.6		1	Y1	342.6		1	Y2	332.3	Sn5:	1	Ni2	261.2
	1	Ni2	334.7	Ni2:	2	Sn1	247.5		2	Sn5	349.5		1	Ni1	263.1
	1	Ni1	342.6		1	Sn4	251.7	Sn2:	1	Ni3	251.0		2	Y2	339.9
Y2:	2	Ni1	310.1		1	Sn5	261.2		2	Sn2	297.4		2	Sn3	343.0
	2	Sn6	312.3		1	Sn6	276.2		1	Y3	313.2		2	Y3	344.1
	2	Sn4	317.7		2	Y3	313.9		2	Sn6	322.3		2	Sn1	349.5
	1	Sn3	321.8		1	Y1	334.7		1	Y2	347.4	Sn6:	2	Ni3	255.7
	1	Sn1	332.3		2	Y2	360.0		2	Y3	354.9		1	Ni2	276.2
	2	Sn5	339.9	Ni3:	1	Sn2	251.0	Sn3:	2	Ni1	251.9		2	Y2	312.3
	1	Sn2	347.4		2	Sn6	255.7		1	Ni1	272.4		1	Y1	317.9
	1	Ni3	350.8		1	Sn4	257.8		1	Sn1	297.4		2	Sn2	322.3
	2	Ni2	360.0		1	Sn1	264.7		2	Y1	312.0		2	Sn1	324.5
Y3:	1	Sn2	313.2		2	Y3	323.0		1	Y1	315.4		1	Y3	342.9
	2	Ni2	313.9		2	Y1	325.0		1	Y2	321.8				
	2	Sn4	316.0		1	Y2	350.8		2	Sn3	326.3				
	2	Ni3	323.0						2	Sn5	343.0				
	1	Sn1	324.6												
	1	Sn6	342.9												
	2	Sn5	344.1												
	2	Sn2	354.9												

Table 5. Fitting parameters of ^{119}Sn *Mössbauer* measurements for YNi_xSn_2 ($x = 0, 0.1, 0.2, 1$). Numbers in parentheses represent the statistical errors in the last digit. δ Isomeric shift; ΔE_Q electric quadrupole splitting; Γ experimental line width

Sample	δ	ΔE_Q/mm s^{-1}	Γ/mm s^{-1}
YSn_2	2.26(8)	1.18(2)	1.00(3)
$YNi_{0.1}Sn_2$	2.17(7)	1.21(5)	0.87(3)
$YNi_{0.2}Sn_2$	2.11(5)	1.26(6)	1.04(2)
$YNiSn_2$	2.11(4)	1.25(4)	1.06(1)

^{119}Sn Mössbauer Spectroscopy

A $Ca^{119m}SnO_3$ source was available for the ^{119}Sn *Mössbauer* spectroscopic investigations. The samples were placed within thin-walled *PVC* containers at a thickness of about 10 mg Sn/cm^2. A palladium foil of 0.05 mm thickness was used to reduce the tin K X-rays concurrently emitted by this source. The measurements were conducted in the usual transmission geometry at 78 K. The spectra were fitted according to the *Levenberg-Marquard* algorithm, leading to the isomer shift (δ), electric quadrupole splitting (ΔE_Q), and experimental line width (Γ) parameters.

Acknowledgements

We are indebted to *B. Heying*, Dipl.-Ing. *U.C. Rodewald*, and Dr. *R.-D. Hoffmann* for the intensity data collections. This work was financially supported by the Deutsche Forschungsgemeinschaft. *C.P.S.* is indebted to the NRW Graduate School of Chemistry for a PhD stipend.

References

[1] Cordey-Hayes M (1964) J Inorg Nucl Chem **26**: 915
[2] Cordey Hayes M (1968) ^{119m}Sn: Inorganic Compounds, Metals, Alloys. In: Goldanskii VI, Herber RH (eds) Chemical Applications of Mössbauer Spectroscopy, chapter 5. Academic Press, New York, pp 314–335
[3] Lippens PE (1999) Phys Rev B **60**: 4576
[4] Asbrand M, Berry FJ, Eisenmann B, Kniep R, Smart LE, Thied RC (1999) Polyhedron **18**: 2427
[5] Hoffmann R-D, Kußmann D, Rodewald UCh, Pöttgen R, Rosenhahn C, Mosel BD (1999) Z Naturforsch **54b**: 709
[6] Lange S, Schappacher FM, Johrendt D, Nilges T, Hoffmann R-D, Pöttgen R (2006) Z Anorg Allg Chem **632**: 1432
[7] Nylén J, Garcìa Garcìa FJ, Mosel BD, Pöttgen R, Häussermann U (2004) Solid State Sci **6**: 147
[8] Hayes CM, Harris IR (1967) Phys Lett **24A**: 80
[9] Sebastian CP, Eckert H, Rayaprol S, Hoffmann R-D, Pöttgen R (2006) Solid State Sci **8**: 560
[10] Sebastian CP, Eckert H, Fehse C, Wright JP, Attfield JP, Johrendt D, Rayaprol S, Hoffmann R-D, Pöttgen R (2006) J Solid State Chem **179**: 2376
[11] Sebastian CP, Fehse C, Eckert H, Hoffmann R-D, Pöttgen R (2006) Solid State Sci, in press
[12] Iandelli A, Palenzona A (1966) Atti Accad Nazl Lincei Rend **40**: 623
[13] Schmidt FA, McMasters OD (1968) J Less-Common Met **15**: 1
[14] Borzone G, Borsese A, Ferro R (1983) Z Anorg Allg Chem **501**: 199
[15] Pöttgen R, Gulden Th, Simon A (1999) GIT Labor Fachzeitschrift **43**: 133
[16] Yvon K, Jeitschko W, Parthé E (1977) J Appl Crystallogr **10**: 73
[17] Cotter PG, Kohn JA, Potter RA (1956) J Am Ceram Soc **39**: 11
[18] Bodak OI, Gladyshevskii EI (1970) Sov Phys Crystallogr **14**: 859
[19] Komarovskaya LP, Aksel'rud LG, Skolozdra RV (1983) Kristallografiya **28**: 1201
[20] Sheldrick GM (1997) SHELXS-97, Program for the Determination of Crystal Structures, University of Göttingen
[21] Sheldrick GM (1997) SHELXL-97, Program for Crystal Structure Refinement, University of Göttingen
[22] Donohue J (1974) The Structures of the Elements. Wiley, New York
[23] Skolozdra RV (1997) Stannides of Rare Earth and Transition Metals. In: Gschneidner KA Jr, Eyring L (eds) Handbook on the Physics and Chemistry of Rare Earths, vol 24, chapter 164. Elsevier, Amsterdam, pp 399–517
[24] Emsley J (1999) The Elements. Oxford University Press, Oxford
[25] Dörrscheidt W, Savelsberg G, Stöhr J, Schäfer H (1982) J Less-Common Met **83**: 269
[26] Villars P, Calvert LD (1991) Pearson's Handbook of Crystallographic Data for Intermetallic Phases, Second Edition, American Society for Metals, Materials Park, OH 44073, and (1997) desk edition
[27] Méot-Meyer M, Venturini G, Malaman B, Roques B (1985) Mater Res Bull **20**: 1515
[28] François M, Venturini G, Malaman B, Roques B (1990) J Less-Common Met **160**: 197
[29] Venturini G, François M, Malaman B, Roques B (1990) J Less-Common Met **160**: 215
[30] Das I, Sampathkumaran EV (1992) Solid State Commun **83**: 765
[31] Das I, Sampathkumaran EV, Hirota K, Ishikawa M (1994) Phys Rev B **49**: 3586
[32] Das I, Sampathkumaran EV (1995) Physica B **205**: 259
[33] Lukachuk M, Rodewald UCh, Zaremba VI, Hoffmann R-D, Pöttgen R (2004) Z Anorg Allg Chem **630**: 2253
[34] Pöttgen R, Simon A (1996) Z Anorg Allg Chem **622**: 779
[35] Bhan Z, Sikirica M (1965) Acta Crystallogr **18**: 594
[36] Parthé E, Chabot B (1984) Crystal Structuress and Crystal Chemistry of Ternary Rare Earth-Transition Metal Borides, Silicides and Homologues. In: Gschneidner KA Jr, Eyring L (eds) Handbook on the Physics and Chemistry of Rare Earths, vol 6. North-Holland, Amsterdam, pp 113–334
[37] Cenzual K, Parthé E (1984) Acta Crystallogr C **40**: 1127
[38] Parthé E, Chabot B, Cenzual K (1985) Chimia **39**: 164